Chebyshev polynomial representation of imaginary-time response functions

Emanuel Gull,[1] Sergei Iskakov,[1] Igor Krivenko,[1] Alexander A. Rusakov,[2] and Dominika Zgid[2]
[1]*Department of Physics, University of Michigan, Ann Arbor, Michigan 48109, USA*
[2]*Department of Chemistry, University of Michigan, Ann Arbor, Michigan 48109, USA*

(Received 6 May 2018; published 15 August 2018)

Problems of finite-temperature quantum statistical mechanics can be formulated in terms of imaginary (Euclidean) -time Green's functions and self-energies. In the context of realistic Hamiltonians, the large energy scale of the Hamiltonian (as compared to temperature) necessitates a very precise representation of these functions. In this paper, we explore the representation of Green's functions and self-energies in terms of a series of Chebyshev polynomials. We show that many operations, including convolutions, Fourier transforms, and the solution of the Dyson equation, can straightforwardly be expressed in terms of the series expansion coefficients. We then compare the accuracy of the Chebyshev representation for realistic systems with the uniform-power grid representation, which is most commonly used in this context.

DOI: 10.1103/PhysRevB.98.075127

I. INTRODUCTION

The equilibrium properties of interacting quantum systems at finite temperature can be described by the Matsubara formalism of quantum statistical mechanics [1]. In this formalism, single- and two-particle quantities are expressed in terms of Green's functions, self-energies, susceptibilities, and vertex functions in imaginary time.

The imaginary-time formalism has a long tradition in the calculation of properties of interacting systems [2,3], and weak-coupling methods such as the random-phase approximation [4,5], the self-consistent second-order approximation [6–12], or the GW method [13] can be formulated in terms of imaginary-time Green's functions and self-energies. Numerical algorithms, including lattice Monte Carlo methods [14], impurity solver algorithms [15–19], and diagrammatic Monte Carlo methods [20], are similarly based on the finite-temperature Green's function formalism, as are some implementations of the dynamical mean-field theory [21] and its extensions [22–24].

Finite-temperature fermionic (bosonic) imaginary-time Green's functions are antiperiodic (periodic) functions with period β and can be reduced to the interval $[0, \beta]$. In most of the applications mentioned above, they are sampled on a uniform grid, typically with 10^2-10^4 grid discretization points. However, a uniform representation of the function is only efficient in effective model systems. In large multiorbital systems, and especially in systems with realistic band structures, an accurate representation of Green's functions with a uniform discretization would require millions to billions of time slices per Green's function element, as the wide energy spacing of realistic Hamiltonians results in features on very small time scales. Therefore, more compact representations of Green's functions are needed in this context.

A first attempt at constructing a more compact representation, the "uniform power mesh," was proposed by Ku [25]; see also Ref. [26]. There, a set of logarithmically spaced nodes is chosen on the imaginary-time interval. The Green's function is then uniformly discretized between those nodes, using a constant number of points for each interval. This leads to a clustering of points near 0 and β, where much of the rapid change of Green's functions for low-lying excitations takes place. Later, Legendre polynomial representations [27] were pioneered in the context of continuous-time Monte Carlo methods, where the compactness of the representation could reduce the number of observables that needed to be accounted for, and in the context of analytical continuation [28], where an intermediate basis of a singular value decomposed analytic continuation kernel [29] could further reduce the number of coefficients. This was followed by progress in the context of perturbation methods for realistic systems [9], where the combination of uniform power meshes and Legendre polynomial expansions drastically reduced the size of the imaginary-time grid. In Matsubara frequency space, Ref. [10] showed that much of the Matsubara frequency dependence of Green's functions and self-energies can be represented by interpolation functions, thereby vastly reducing the number of frequencies required to obtain accurate results.

For practical use in real materials simulations, a set of basis functions for imaginary-time Green's functions and self-energies should satisfy at least the following criteria. First and foremost, it should be possible to represent the large energy spread of typical interacting systems with a small number of coefficients. Second, it should be straightforward to confirm that the representation is fully converged, i.e., that basis truncation errors are small. Finally, the mathematics of performing typical operations on Green's functions, such as evaluating a self-energy, a polarization bubble, a Dyson equation, or Fourier transforming data to frequency space and evaluating energies should be straightforward, both analytically and in terms of the numerical effort.

The representations mentioned above satisfy some but not all of these requirements. In this paper, we therefore introduce an alternative representation of imaginary-time Green's functions, based on approximating the Green's functions by a sum of scaled Chebyshev polynomials of the first kind. We test the performance of this expansion explicitly for a variety

 ©2018 American Physical Society

of systems in realistic basis sets, including periodic solids. We examine how the number of coefficients converges as a function of temperature, basis-set size, and precision required, and we show how Fourier transforms and Dyson equations can be solved directly in Chebyshev space.

The remainder of this paper is organized as follows. In Sec. II, we present the detailed derivation of the method. In Sec. III, we list and discuss the numerical results of our method as applied to realistic molecular and solid-state calculations. We present conclusions in Sec. IV.

II. METHOD

A. Chebyshev expansion of response functions

Imaginary-time Green's functions $G^{\nu\mu}(\tau) = -\langle c_\nu(\tau) c^\dagger_\mu(0)\rangle$ are defined for $0 \leqslant \tau \leqslant \beta$, where β is the inverse temperature, and Greek letters correspond to orbital indices. Outside this interval, fermionic Green's functions satisfy β antiperiodicity $G(-\tau) = -G(\beta - \tau)$, whereas bosonic response functions are β-periodic, $\chi(-\tau) = \chi(\beta - \tau)$. In the following, we will work on the interval $[0, \beta]$, and we use the mapping $x(\tau) = \frac{2\tau}{\beta} - 1$ to map it to the interval $[-1, 1]$.

The Chebyshev polynomials of the first kind, $T_j(x)$ [30], form a complete basis for bounded functions in this interval. Any Green's function, or other response function can therefore be expanded into a sum of Chebyshev polynomials and approximated by a truncated Chebyshev series

$$G^{\nu\mu}(x) \approx \sum_{j=0}^{m}{}' g_j^{\nu\mu} T_j(x) = \sum_{j=0}^{m} g_j^{\nu\mu} T_j(x) - \frac{1}{2} g_0^{\nu\mu}, \tag{1}$$

$$g_j^{\nu\mu} = \frac{2}{\pi} \int_{-1}^{1} \frac{G^{\nu\mu}(x) T_j(x)}{\sqrt{1-x^2}} dx. \tag{2}$$

The primed sum denotes the special treatment of the coefficient g_0 customary in this context [31]. Based on the discrete orthogonality properties of the Chebyshev polynomials [31], if the values of $G^{\nu\mu}(x)$ are known at the zeros of the mth Chebyshev polynomial, $x_k = \cos\left(\frac{2k-1}{2m}\pi\right)$, $k = 1, \ldots, m$, the calculation of the coefficients in Eq. (2) simplifies to a discrete cosine transform. In addition, values of the Chebyshev approximant anywhere in the interval $0 \leqslant \tau \leqslant \beta$ can be obtained from $g_j^{\nu\mu}$ using Clenshaw recursion relations [32].

Chebyshev representations are particularly efficient for approximating analytic functions on the interval $[-1, 1]$, as approximation theory guarantees that the magnitude of the coefficients $g_j^{\nu\mu}$ decays at least exponentially as $j \to \infty$, and that the maximum difference between G and its Chebyshev approximant decreases exponentially [30]. The fermionic and bosonic imaginary-time Green's functions, polarization functions, self-energies, and response functions appearing in finite-temperature many-body theory are all analytic functions between 0 and β.

As we will show in Sec. III, fast convergence of Green's functions and self-energies with the number of Chebyshev coefficients is observed, and the discrete cosine transforms and recursion relations allow for quick numerical operations on the data in practice. We find that our examples converge to a precision of 10^{-10} within about 40 coefficients for the simple realistic systems, such as hydrogen molecules, whereas around 500 Chebyshev nodes are required to describe a krypton atom in a pseudopotential approximation.

B. Convolutions

Products of Matsubara Green's functions correspond to convolutions in imaginary time. The convolution

$$A(t) = \int_0^\beta d\tau\, B(t-\tau) C(\tau), \tag{3}$$

with A, B, and C Green's functions or self-energies, requires careful treatment of the discontinuity of $B(t-\tau)$ at $t = \tau$, so that standard Chebyshev convolution formulas [33] cannot be applied. Instead, we express Eq. (3) by expanding the rescaled integral into Chebyshev components (appropriately rescaling the zero coefficients)

$$\sum_j{}' a_j^{\nu\mu} T_j(x) = \sum_{kl\xi} b_k^{\nu\xi} c_l^{\xi\mu} I_{kl}(x), \tag{4}$$

$$I_{kl}(x) = \frac{\beta}{2}\left[\int_{-1}^{x} T_k(x-y-1) T_l(y) dy \mp \int_{x}^{1} T_k(x-y+1) T_l(y) dy\right], \tag{5}$$

where the minus (plus) sign corresponds to a convolution of fermionic (bosonic) functions, and $I_{kl}(x)$ is an integral of polynomials in $[-1, 1]$ and can therefore be written as a Chebyshev series,

$$I_{kl}(x) = \frac{\beta}{2} \sum_j{}' t_{kl}^j T_j(x), \tag{6}$$

resulting in the formulation of the fermionic convolution as a matrix multiplication,

$$a_j^{\nu\mu} = \frac{\beta}{2} \sum_{kl\xi} b_k^{\nu\xi} c_l^{\xi\mu} t_{kl}^j. \tag{7}$$

This representation becomes more efficient than the Fourier representation whenever a very large number of Fourier components is required. A detailed derivation of recursion relations for bosonic and fermionic integrals t_{kl}^j is provided in the Appendix.

C. Dyson equation

Most diagrammatic algorithms are formulated in imaginary time, where the interaction vertex V_{pqrs} is instantaneous. However, most contain a step for solving a Dyson equation, either for adjusting a chemical potential to the desired particle number or to obtain self-consistent propagators. This Dyson equation $G = G_0 + G_0 \Sigma G$ is most conveniently expressed in frequency space, where it can be solved for each frequency independently. In imaginary time, the Dyson equation determining G, given G_0 and Σ, corresponds to a Fredholm integral equation of the second kind [34,35]. As in the case of the Fourier transforms and convolutions, the discontinuity at zero and the highly nonuniform nature of the Green's functions make uniform discretizations [6] inefficient. Defining

$B(t) = \int d\tau\, G_0(t-\tau)\Sigma(\tau)$ and expanding into Chebyshev coefficients, we obtain the equation

$$g_j^{\nu\mu} = g_{(0)j}^{\nu\mu} + \frac{\beta}{2}\sum_{kl\xi} b_k^{\nu\xi} g_l^{\xi\mu} t_{kl}^j \tag{8}$$

with t_{kl}^j defined as above. This linear system can be recast as $\sum_{j\xi} A_{ij}^{\nu\xi} g_j^{\xi\mu} = g_{0i}^{\nu\mu}$ with a matrix $A_{ij}^{\nu\mu} = \delta_{ij}\delta_{\nu\mu} - \frac{\beta}{2}\sum_k b_k^{\nu\mu} t_{kl}^j$. The solution of the Fredholm integral equation is thereby mapped onto the solution of a system of linear equations, bypassing the Matsubara domain entirely.

D. Fourier transforms

Fourier transforms between time and frequency domains require a careful treatment of the Green's function around $\tau = 0$. At this point, fermionic Green's functions are discontinuous due to the fermion anticommutation relation. This discontinuity is usually absorbed in an explicit treatment of the short-time (high-frequency) behavior using high-frequency expansions and suitable model functions [19,36,37]. Even with this high-frequency treatment, the number of Matsubara frequencies required for accurate energies and spectra of realistic systems at low temperature is very large. This is because the spacing of the Matsubara points is given by the temperature, whereas the location of the main features of the function is given by the energy scale of the Hamiltonian. In realistic systems, these energy scales are different by many orders of magnitude, requiring millions to billions of frequency points. Adaptive grids, such as the one developed in Ref. [10], provide a partial solution to this problem.

Fourier transforms of Chebyshev polynomials to Matsubara frequencies $\omega_n = \frac{(2n+\zeta)\pi}{\beta}$ ($\zeta = 0$ for bosons and $\zeta = 1$ for fermions) are obtained by evaluating the integral [38]

$$\begin{aligned}\mathcal{F}(T_m)(i\omega_n) &= \int_0^\beta d\tau\, T_m(x(\tau)) e^{i\omega_n\tau} \\ &= \frac{\beta}{2}\int_{-1}^1 dx\, T_m(x) e^{i\lambda_n\frac{x+1}{2}} = F_{mn}^\zeta\end{aligned} \tag{9}$$

for dimensionless Matsubara frequencies $\lambda_n = (2n+\zeta)\pi$. In the special case of bosonic Matsubara frequency zero, we find that

$$F_{m0}^0 = \frac{\beta}{2}\int_{-1}^1 dx\, T_m(x) = \frac{\beta}{2}\begin{cases}\frac{1+(-1)^m}{1-m^2}, & m \neq 1, \\ 0, & m = 1.\end{cases} \tag{10}$$

For all nonzero λ_n, partial integration yields

$$\begin{aligned}I_m^\zeta(n) = \int_{-1}^1 dx\, T_m(x) e^{i\lambda_n\frac{x+1}{2}} &= \frac{2}{i\lambda_n} e^{i\lambda_n\frac{x+1}{2}} T_m(x)\Big|_{-1}^1 \\ &- \frac{2}{i\lambda_n}\int_{-1}^1 dx\, T_m'(x) e^{i\lambda_n\frac{x+1}{2}},\end{aligned} \tag{11}$$

where the boundary term evaluates to

$$\frac{2}{i\lambda_n} e^{i\lambda_n\frac{x+1}{2}} T_m(x)\Big|_{-1}^1 = 2i\frac{(-1)^m - (-1)^\zeta}{\lambda_n}. \tag{12}$$

Using $T_m'(x) = mU_{m-1}(x)$, where $U_m(x)$ are Chebyshev polynomials of the second kind related to $T_m(x)$ via

$$U_m(x) = \begin{cases}2\left(\sum_{j\ \text{odd}}^m T_j(x)\right), & m \text{ odd}, \\ 2\left(\sum_{j\ \text{even}}^m T_j(x)\right) - 1, & m \text{ even},\end{cases} \tag{13}$$

we transform the second integral in (11) as

$$\begin{aligned}\frac{2}{i\lambda_n}\int_{-1}^1 dx\, T_m'(x) e^{i\lambda_n\frac{x+1}{2}} &= \frac{2m}{i\lambda_n}\int_{-1}^1 U_{m-1}(x) e^{i\lambda_n\frac{x+1}{2}} \\ &= \frac{2m}{i\lambda_n}\int_{-1}^1 dx\, e^{i\lambda_n\frac{x+1}{2}}\begin{cases}2\sum_{j,\text{odd}}^{m-1} T_j(x), & m \text{ even}, \\ 2\sum_{j,\text{even}}^{m-1} T_j(x) - 1, & m \text{ odd}.\end{cases}\end{aligned} \tag{14}$$

This results in a recursion relation with respect to index m,

$$\begin{aligned}I_m^\zeta(n) = 2i\frac{(-1)^m - (-1)^\zeta}{\lambda_n} \\ + \frac{2im}{\lambda_n}\begin{cases}2\left(\sum_{j\ \text{odd}}^{m-1} I_j^\zeta(n)\right), & m \text{ even}, \\ 2\left(\sum_{j\ \text{even}}^{m-1} I_j^\zeta(n)\right) - I_0^\zeta(n), & m \text{ odd},\end{cases}\end{aligned} \tag{15}$$

which we start by explicitly computing $I_0^0(n) = 2\delta_{n,0}$ or $I_0^1(n) = 4i/\lambda_n$. This recursion relation is unstable [39] and therefore has to be implemented in high-precision arithmetic. With Eq. (9) we then write the Fourier transform as

$$\mathcal{F}(G)(i\omega_n) = \sum_j g_j F_{jn}^\zeta, \tag{16}$$

where the Fourier matrix F_{jn}^ζ is computed once and tabulated. The inverse transform is done by evaluating the function at the Chebyshev nodes and using a discrete cosine transform to obtain the corresponding coefficients.

Accurate Fourier transforms and energy evaluations in Fourier space require high-frequency expansion coefficients for the Green's function to at least third order, so that $G(i\omega_n) = \frac{c_1}{i\omega_n} + \frac{c_2}{(i\omega_n)^2} + \frac{c_3}{(i\omega_n)^3} + O(i\omega_n^{-4})$. Fourier transform of the Green's function implies that $c_1 = -[G(0^+) + G(\beta^-)]$, $c_2 = G'(0^+) + G'(\beta^-)$, and in general $c_{k+1} = (-1)^{k+1}[G^{(k)}(0^+) + G^{(k)}(\beta^-)]$. These expansion coefficients are available to any order due to the identities

$$\left.\frac{d^p T_n}{dx^p}\right|_{x=\pm1} = (\pm1)^{n+p}\prod_{k=0}^{p-1}\frac{n^2-k^2}{2k+1}, \tag{17}$$

and in particular

$$\left.\frac{dT_n}{dx}\right|_{x=\pm1} = (\pm1)^n n^2, \tag{18}$$

$$\left.\frac{d^2 T_n}{dx^2}\right|_{x=\pm1} = (\pm1)^n\frac{n^4-n^2}{3}. \tag{19}$$

III. RESULTS

To demonstrate the efficiency of the proposed method, we consider four test systems. To make the results reproducible, we use electronic structure systems in standardized basis sets

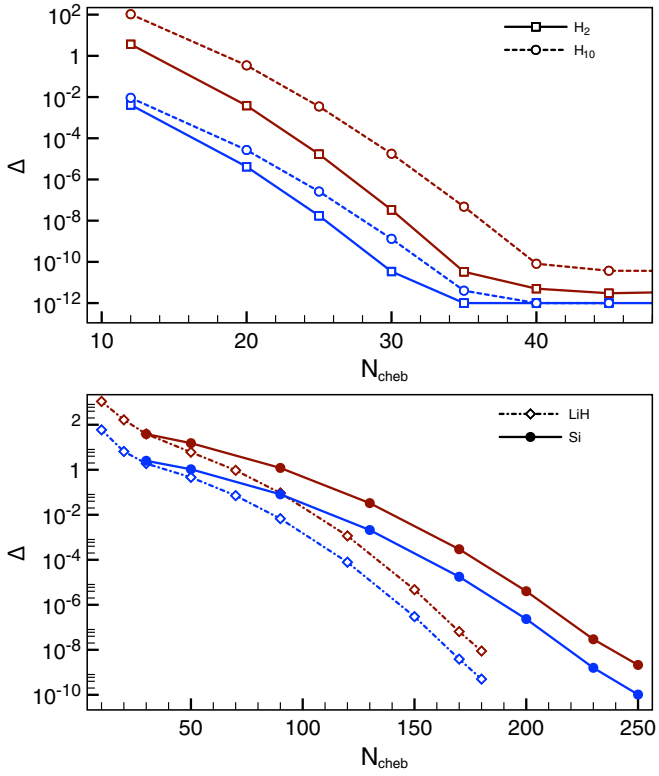

FIG. 1. Convergence of the Hartree-Fock Green's function with the number of Chebyshev polynomials. Red curves correspond to the sum of all differences with respect to the exact result. Blue curves correspond to the maximum difference when compared to the exact result. Top panel: H_2 molecule (open square) and H_{10} molecule (open circle). Bottom panel: periodic one-dimensional LiH (open diamond) and three-dimensional Si crystal (filled circle). Parameters as specified in Table I.

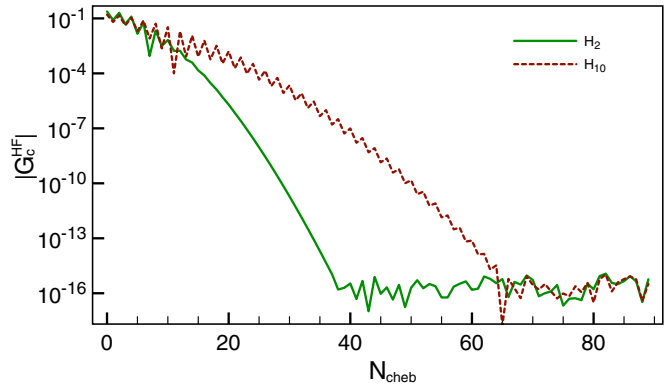

FIG. 2. Exponential decay of the Chebyshev coefficients for the Hartree-Fock Green's function. H_2 molecule (green) and H_{10} molecule (red, dashed) with parameters as specified in Table I.

that are well documented [40] and readily available [41,42]. The first two systems are hydrogen molecules, both as H_2 and as a one-dimensional chain of ten hydrogen atoms. We use the minimal STO-3g basis [43] and place the atoms at an interatomic distance of $d = 1.5$ Å. These cases are chosen as "easy" examples of realistic calculations. We also consider two periodic systems. First, a one-dimensional periodic LiH solid in the triple-zeta quality basis set (pob-TZVP) from Ref. [44], and second, a three-dimensional Si crystal in the following basis set: the innermost $1s$, $2s$, and $2p$ shells are replaced with the LANL2DZ effective core potentials [45–47], while the basis functions for the outer $3s$, $3p$, and $3d$ shells are taken from the Si_88-31G*_nada_1996 basis [48–50]. All systems were evaluated at an inverse temperature of $\beta = 100$ Ha^{-1}. The detailed parameters are shown in Table I.

The exponential convergence predicted by theory can be observed in practice. Figure 1 shows the convergence of the Chebyshev Green's function to the exactly evaluated Hartree-Fock solution as a function of the number of coefficients. Shown is the difference Δ between the interpolated Green's function and a reference Green's function evaluated analytically on a uniform-power grid (with 15 power points and 18 uniform points between each pair of power points) as a function of the number of coefficients, both as the maximum deviation (dark red curves) and as the sum of all deviations at all points (blue curves).

It is evident that the Chebyshev approximation converges to the exactly evaluated Hartree-Fock solution as a function of the number of expansion coefficients, until numerical roundoff errors are reached at a precision of 10^{-12}. For the hydrogen systems used here, between 30 and 40 coefficients lead to a maximum uncertainty of around 10^{-10}. More complex systems require more coefficients, as illustrated by the one-dimensional LiH and three-dimensional Si, which only reach a precision of 10^{-8} within 180 and 230 coefficients, respectively (lower panel of Fig. 1). This convergence stems from the fast decay of the Chebyshev expansion coefficients. Figure 2 illustrates this point by showing the maximum magnitude of the Chebyshev coefficients of a given polynomial order as a function of order. There, the noise floor is reached for around 40 (H_2) or 80 (H_{10}) coefficients, at a coefficient size of around 10^{-16}.

Figure 3 shows the number of Chebyshev coefficients required to reach a predetermined precision as temperature is varied. The top panel analyzes the Hartree-Fock Green's function as the temperature is lowered, while the bottom panel analyzes the second-order self-energy. The systems used are a linear chain of ten hydrogen atoms in the STO-3g basis and a periodic one-dimensional arrangement of LiH, both systems with parameters chosen as in Table I. For the systems illustrated here, the log-log axes suggest a power-law behavior, and a square-root fit shows that the scaling as a function of temperature grows slower than $\sim T^{-1/2}$, similar to observations in the context of model calculations in a Legendre basis [51].

The number of Chebyshev points required is strongly system-dependent, and depends in particular on the energy spread of the atomic orbitals. This is illustrated in the top panel of Fig. 4, which shows the maximum and total difference between an exactly evaluated Hartree-Fock Green's function and its Chebyshev approximant for a Kr atom as a function of the number of coefficients. One can see that, for the bases chosen, the maximum error remains $\sim 10^{-4}$ even when 700 components are chosen, independent of the basis. This slow convergence is due to low-lying core states, which are fully occupied and in the τ-domain represented as an exponential decay toward zero with a large decay constant.

TABLE I. Geometries and basis sets for the systems used. All systems were evaluated at an inverse temperature of $\beta = 100\ \mathrm{Ha}^{-1}$.

Molecular systems			
	Basis	Interatomic distance (Å)	
H_2	STO-3g	1.5000	
H_{10}	STO-3g	1.5000	
Periodic systems			
	Basis	Unit-cell coordinates (Å)	Translation vectors (Å)
LiH	pob-TZVP	Li 0.0 0.0 0.0 H 1.671286 0.0 0.0	(3.342572, 0.0, 0.0)
Si	Custom, see text	Si 0.0000 0.0000 0.0000 Si 1.3575 1.3575 1.3575	(0.0, 2.7150, 2.7150) (2.7150, 0.0, 2.7150) (2.7150, 2.7150, 0.0)

Alternatively, choosing effective core potentials (lower panel of Fig. 4) eliminates these low-lying states and causes a more rapid convergence of the polynomial expansion with the number of coefficients (maximum difference of 10^{-9} at ∼450 coefficients). Whether a different treatment of the core states, for example by analytically modeling them with a δ function in real frequency, is more effective than a brute force expansion into Chebyshev polynomials is an open question for future research.

To contrast these results with the commonly used uniform power grids, Fig. 5 shows the convergence of power grid data to the exact result for the periodic one-dimensional LiH solid of Fig. 1 (lower panel). Data on the power grid are interpolated using cubic splines. This leads to a convergence $\sim u^{-4}$ as a function of the uniform spacing u. It is evident that there is an "optimal" number of power points (12, in this case), which minimizes the prefactor of the convergence to the exact result (but does not change the scaling). For results accurate to 10^{-8}, 350 τ-points were necessary for the optimal choice of power grid parameters, around twice as many as for the Chebyshev grid.

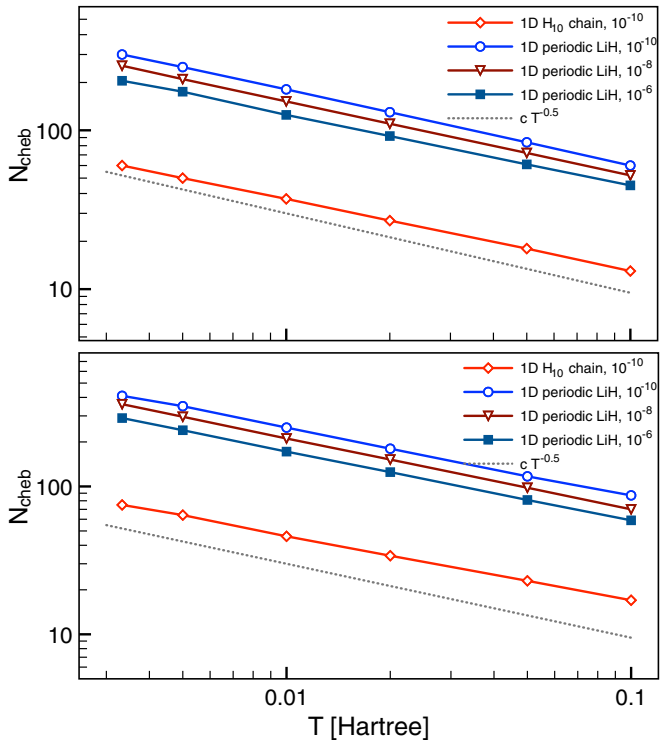

FIG. 3. Number of Chebyshev coefficients required to resolve the Hartree-Fock Green's function (top panel) and the bare second-order self-energy (bottom panel) at temperature T measured in Hartree up to the precision indicated, for one-dimensional H_{10} and one-dimensional periodic LiH. Parameters as specified in Table I.

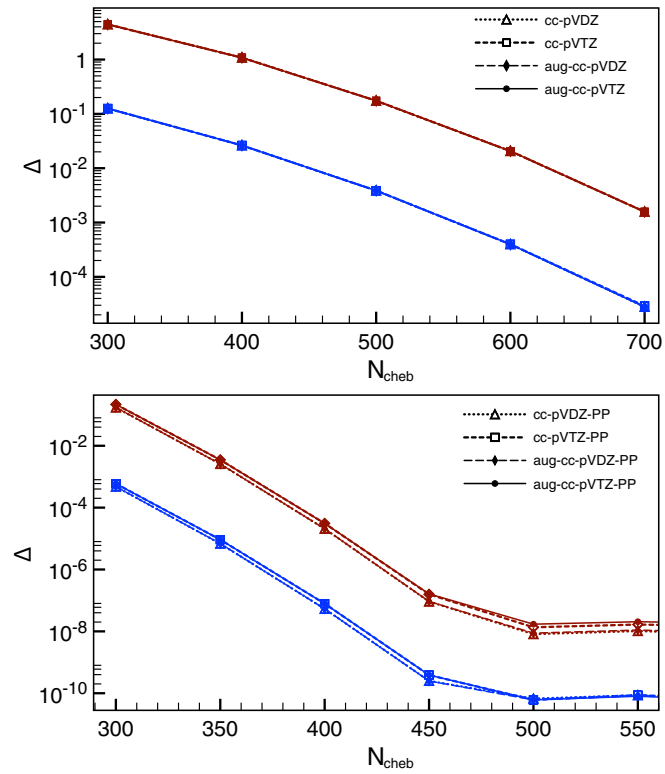

FIG. 4. Total (red) and maximum (blue) difference between the Chebyshev Green's function and the exact Hartree-Fock Green's function as a function of the number of Chebyshev coefficients for a krypton atom in four different basis sets [42,52,53] without (top panel) and with (bottom panel) effective core potentials.

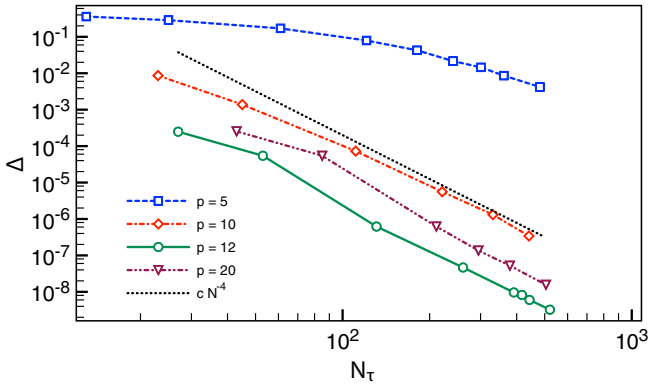

FIG. 5. Convergence of the power grid interpolation of a Hartree-Fock Green's function with the total number of points in the grid for the periodic one-dimensional LiH solid. p denotes the power discretization of the grid; parameters as specified in Table I.

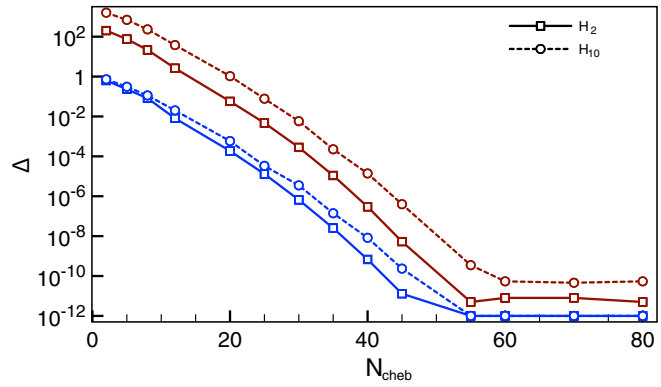

FIG. 7. Convergence of the Dyson equation solution for H_2 and H_{10} with the number of Chebyshev polynomials with parameters specified in Table I. Red lines: sum of errors. Blue lines: maximum error. Squares: H_2. Circles: H_{10}.

The full power of the Chebyshev representation becomes apparent when Fourier integrals or a solution of the Dyson equation have to be computed for data known in the imaginary-time domain. Figure 6 shows the convergence of the solution of the Dyson equation using trapezoidal integration in imaginary time, as originally proposed in Ref. [54]. The system studied is H_2 in the STO-3g basis, and discrete imaginary-time points are defined on a power grid with different numbers of power points. The precision of this method is limited by the convergence rate of the trapezoidal integration of the uniform part, which is only quadratic, such that even with 500 time slices, only a precision of roughly 10^{-4} can be achieved. In contrast, Fig. 7 shows that with the method introduced in this paper, convergence is faster than exponential. Using around 50 slices, a precision close to 10^{-10} can be reached.

Similar behavior is obtained whenever Fourier integrals need to be computed from a uniform-power grid (not shown here). Data are usually first interpolated by a spline onto a uniform grid and then Fourier-transformed to Matsubara frequencies using a fast Fourier transform. The convergence of the spline to the exact result is the leading contribution to the error of the transform and leads to inaccuracies in the intermediate- to high-frequency region. In contrast, the closed form of Eq. (16) avoids this interpolation step entirely.

Finally, we summarize the different aspects of basis functions for imaginary-time Green's functions in Table II. The comparison is subjective by nature, and the suitability of a given basis set will very much depend on the application. We list the compactness (or suitability for large realistic systems), the cost of constructing the basis set (cheap or expensive), the ways of evaluating arbitrary imaginary-time points (via interpolation, recursion, analytic continuation formula, fast Fourier transform, or nonequidistant FFT), the ways of evaluating Matsubara points, and the preferred (or so far tested) ways of solving the Dyson equation.

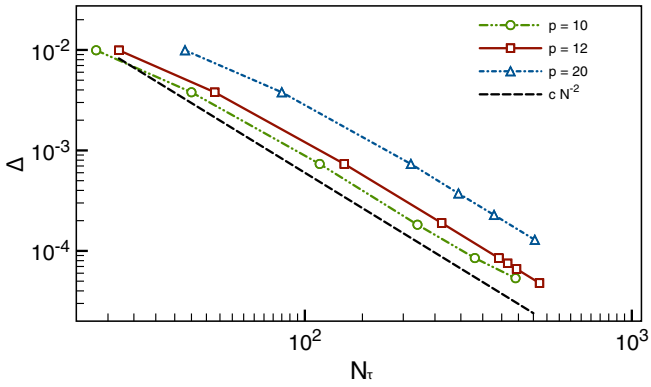

FIG. 6. Convergence of the Dyson equation solution for the H_2 molecule in discretized imaginary time using the method proposed in Ref. [54]. p denotes the number of power points of the grid, and parameters are as specified in Table I.

IV. CONCLUSIONS

In conclusion, we have explored the use of an orthogonal polynomial basis for imaginary-time Green's functions in the context of realistic materials. We have observed the exponential convergence guaranteed by the analytic nature of Green's functions in practice, and we showed that for typical systems, substantially fewer imaginary-time points are needed than for a uniform-power grid. The convergence rate of the expansion

TABLE II. Subjective comparison of different aspects of the various basis sets for finite-T Green's functions. The basis sets vastly differ in their Compactness (Comp.), basis construction effort (Const.), way of evaluating imaginary time (Imag.) or Matsubara (Mat.) Green's function values, and ways of solving the Dyson equation (via Fourier to Matsubara space, where the equation is diagonal, or as described in the main text).

Basis	Comp.	Const.	Imag	Mat.	Dyson
Uniform	No	cheap	interp.	FFT	Fourier
Power	No	cheap	interp.	Fourier	Fourier
Chebyshev	Yes	cheap	Recursion	Sec. II D	Sec. II C
Legendre	∼Yes	cheap	Recursion	Ref. [27]	Fourier
IR [29]	Very	exp.	ac	ac	ac
Matsubara	No	cheap	FFT		diag.
Spline [9]	∼Yes	exp.	NFFT	interp.	diag.

depends on the system. While low-lying core states present a difficulty for this basis and lead to a slow convergence of the expansion, the complex spectral behavior near the chemical potential is well captured by the first 50–100 coefficients in the systems examined here. We have also shown that convolutions, Dyson equations, and Fourier transforms, which correspond to commonly used operations on imaginary-time Green's functions, can be performed accurately and efficiently. This paves the way for using Chebyshev approximated imaginary-time Green's functions in calculations of realistic and model systems, replacing the uniform and uniform-power grids that have so far been used in this context.

ACKNOWLEDGMENTS

E.G. and S.I. were supported by the Simons Foundation via the Simons Collaboration on the Many-Electron Problem. I.K. was supported by DOE ER 46932, and D.Z. and A.A.R. were supported by NSF-CHE-1453894. This research used resources of the National Energy Research Scientific Computing Center, a DOE Office of Science User Facility supported by the Office of Science of the U.S. Department of Energy under Contract No. DE-AC02-05CH11231.

APPENDIX A: CONVOLUTION OF CHEBYSHEV POLYNOMIALS AND t-COEFFICIENTS

Chebyshev interpolation can be used to solve Fredholm integral equations with piecewise-continuous convolution kernels. The solution of such problems requires knowledge of a special system of coefficients t_{kl}^{j} defined according to

$$T_{kl}(x) = {\sum_{j}}' t_{kl}^{j} T_j(x), \tag{A1}$$

$$T_{kl}(x) = T_{kl}^{-}(x) \pm T_{kl}^{+}(x), \tag{A2a}$$

$$T_{kl}^{-}(x) \equiv \int_{-1}^{x} T_k(x-\tau-1)T_l(\tau)d\tau, \tag{A2b}$$

$$T_{kl}^{+}(x) \equiv -\int_{x}^{1} T_k(x-\tau+1)T_l(\tau)d\tau. \tag{A2c}$$

The plus (minus) sign in Eq. (A2c) corresponds to the fermionic (bosonic) Green's function case. In the following derivations, we will use the product formula for $T_m(x)$:

$$T_m(x)T_n(x) = \tfrac{1}{2}\big[T_{m+n}(x) + T_{|m-n|}(x)\big], \tag{A3}$$

and, in particular, its special case of $n = 1$,

$$T_{m+1}(x) = 2xT_m(x) - T_{|m-1|}(x). \tag{A4}$$

The Chebyshev polynomials $T_m(x)$ form an orthogonal system of functions on segment $[-1;1]$ with respect to a scalar product,

$$\langle f(x), g(x)\rangle = \int_{-1}^{1} f(x)g(x)\frac{dx}{\sqrt{1-x^2}}, \tag{A5}$$

$$\langle T_m(x), T_n(x)\rangle = \pi\frac{1+\delta_{n,0}}{2}\delta_{m,n}. \tag{A6}$$

The orthogonality property means that two equal Chebyshev polynomial expansions have to be equal order by order.

Another result we will need is the indefinite integral of the Chebyshev polynomials,

$$\int T_n(x)dx = \begin{cases} \frac{1}{2}\left(\frac{T_{n+1}(x)}{n+1} + \frac{T_{n-1}(x)}{n-1}\right) + C, & n \neq 1, \\ \frac{T_2(x)+T_0(x)}{4} + C, & n = 1. \end{cases} \tag{A7}$$

1. Symmetry properties of $T_{kl}(x)$

Theorem 1. Functions $T_{kl}(x)$ are symmetric with respect to their indices, $T_{lk}(x) = T_{kl}(x)$.

Proof.

$$\begin{aligned} T_{lk}^{-}(x) &= \int_{-1}^{x} T_l(x-\tau-1)T_k(\tau)d\tau = \begin{Bmatrix} x-\tau-1 = t \\ dt = -d\tau \end{Bmatrix} \\ &= -\int_{x}^{-1} T_l(t)T_k(x-t-1)dt \\ &= \int_{-1}^{x} T_k(x-t-1)T_l(t)dt = T_{kl}^{-}(x). \end{aligned}$$

Similarly, $T_{lk}^{+}(x) = T_{kl}^{+}(x)$, and, according to definition (A2a), $T_{lk}(x) = T_{kl}(x)$.

Corollary 1.1. t-coefficients are symmetric with respect to their lower indices, $t_{lk}^{j} = t_{kl}^{j}$.

Theorem 2. Functions $T_{kl}(x)$ are either even or odd functions, depending on the value of $k+l$, $T_{kl}(-x) = (-1)^{k+l+1}T_{kl}(x)$.

Proof. Using the symmetry property of Chebyshev polynomials, $T_k(-x) = (-1)^k T_k(x)$, we can write

$$\begin{aligned} T_{kl}^{-}(-x) &= \int_{-1}^{-x} T_k(-x-\tau-1)T_l(\tau)d\tau \\ &= (-1)^k \int_{-1}^{-x} T_k(x+\tau+1)T_l(\tau)d\tau \\ &= \begin{Bmatrix} -\tau = t \\ dt = -d\tau \end{Bmatrix} \\ &= -(-1)^k \int_{1}^{x} T_k(x-t+1)T_l(-t)dt \\ &= (-1)^{k+l+1} \int_{1}^{x} T_k(x-t+1)T_l(t)dt \\ &= -(-1)^{k+l+1} \int_{x}^{1} T_k(x-t+1)T_l(t)dt \\ &= (-1)^{k+l+1} T_{kl}^{+}(x). \end{aligned}$$

Similarly, $T_{kl}^{+}(-x) = (-1)^{k+l+1}T_{kl}^{-}(x)$,

$$\begin{aligned} T_{kl}(-x) &= T_{kl}^{-}(-x) \pm T_{kl}^{+}(-x) \\ &= (-1)^{k+l+1}[T_{kl}^{+}(x) \pm T_{kl}^{-}(x)] = (-1)^{k+l+1}T_{kl}(x). \end{aligned}$$

Corollary 2.1. $t_{kl}^{j} = 0$ for even values of $k+l+j$.

Proof. Chebyshev polynomials $T_k(x)$ are even functions for even k and odd functions for odd k. Therefore, expansion (A1) can contain only even j terms when $T_{kl}(x)$ is even and only odd j terms when $T_{kl}(x)$ is odd. Combining this observation with the proven theorem, we conclude that terms with different parities of $k+l+1$ and j do not contribute to the sum (A1).

2. Recurrence relation for the convolutions $T^{\pm}_{kl}(x)$

Chebyshev polynomials of shifted argument fulfill the following recurrence relation:

$$T_{k+1}(x-\tau\pm1) = 2xT_k(x-\tau\pm1) - 2\tau T_{k+1}(x-\tau\pm1) \pm 2T_{k+1}(x-\tau\pm1) - T_{|k-1|}(x-\tau\pm1).$$

Therefore, integrands in Eqs. (A2b) and (A2c) can be expressed as

$$\begin{aligned} &T_{k+1}(x-\tau\pm1)T_l(\tau) \\ &\quad= 2xT_k(x-\tau\pm1)T_l(\tau) - T_k(x-\tau\pm1)[2\tau T_l(\tau)] \\ &\qquad\pm 2T_k(x-\tau\pm1)T_l(\tau) - T_{|k-1|}(x-\tau\pm1)T_l(\tau) \\ &\quad= 2xT_k(x-\tau\pm1)T_l(\tau) - T_k(x-\tau\pm1) \\ &\qquad\times[T_{l+1}(\tau)+T_{|l-1|}(\tau)] \pm 2T_k(x-\tau\pm1)T_l(\tau) \\ &\qquad- T_{|k-1|}(x-\tau\pm1)T_l(\tau). \end{aligned} \tag{A8}$$

Plugging this into Eq. (A2b) or (A2c), we get a recurrence relation for $T^{\pm}_{k,l}(x)$,

$$\begin{aligned} T^{\pm}_{k+1,l}(x) &= 2xT^{\pm}_{k,l}(x) - T^{\pm}_{k,l+1}(x) \\ &\quad- T^{\pm}_{k,|l-1|}(x) \pm 2T^{\pm}_{k,l}(x) - T^{\pm}_{|k-1|,l}(x), \end{aligned} \tag{A9}$$

with boundary conditions

$$\begin{aligned} T^{-}_{k,0}(x) = T^{-}_{0,k}(x) &= \int_{-1}^{x} T_k(x-\tau-1)d\tau \\ &= \left\{\begin{matrix} x-\tau-1=t \\ dt=-d\tau \end{matrix}\right\} = -\int_{x}^{-1} T_k(t)dt = \int_{-1}^{x} T_k(t)dt, \\ T^{+}_{k,0}(x) = T^{+}_{0,k}(x) &= -\int_{x}^{1} T_k(x-\tau+1)d\tau \\ &= \left\{\begin{matrix} x-\tau+1=t \\ dt=-d\tau \end{matrix}\right\} = \int_{1}^{x} T_k(t)dt = -\int_{x}^{1} T_k(t)dt, \end{aligned}$$

which lead to

$$\begin{aligned} T^{-}_{k,0}(x) &= T^{-}_{0,k}(x) \\ &= \begin{cases} \frac{T_2(x)-T_0(x)}{4}, & k=1, \\ \frac{1}{2}\left(\frac{T_{k+1}(x)+(-1)^k}{k+1} - \frac{T_{|k-1|}(x)+(-1)^k}{k-1}\right), & k\neq 1, \end{cases} \end{aligned} \tag{A10}$$

$$\begin{aligned} T^{+}_{k,0}(x) &= T^{+}_{0,k}(x) \\ &= \begin{cases} \frac{T_2(x)-T_0(x)}{4}, & k=1, \\ \frac{1}{2}\left(\frac{T_{k+1}(x)-1}{k+1} - \frac{T_{|k-1|}(x)-1}{k-1}\right), & k\neq 1, \end{cases} \end{aligned} \tag{A11}$$

or generally

$$\begin{aligned} T^{\pm}_{k,0}(x) &= T^{\pm}_{0,k}(x) \\ &= \begin{cases} \frac{T_2(x)-T_0(x)}{4}, & k=1, \\ \frac{1}{2}\left(\frac{T_{k+1}(x)-(\pm1)^{k+1}}{k+1} - \frac{T_{|k-1|}(x)-(\pm1)^{k-1}}{k-1}\right), & k\neq 1. \end{cases} \end{aligned} \tag{A12}$$

To apply recurrence (A9), one needs expressions for $T_{1,l}(x)$ in addition to the boundary values given above. These can be derived from Eq. (A9) with $k=0$,

$$T_{1,l}(x) = \tfrac{1}{2}\left[2xT^{\pm}_{0,l}(x) - T^{\pm}_{0,l+1}(x) - T^{\pm}_{0,|l-1|}(x) \pm T^{\pm}_{0,l}(x)\right]. \tag{A13}$$

The complete set of equations reads as follows:

$$\begin{aligned} T^{\pm}_{k,0}(x) &= T^{\pm}_{0,k}(x) \\ &= \frac{1}{2}\left(\frac{T_{k+1}(x)-(\pm1)^{k+1}T_0(x)}{k+1} - \frac{T_{|k-1|}(x)-(\pm1)^{k-1}T_0(x)}{k-1}(1-\delta_{k,1})\right), \\ T_{1,l}(x) &= \frac{1}{2}\left[2xT^{\pm}_{0,l}(x) - T^{\pm}_{0,l+1}(x) - T^{\pm}_{0,|l-1|}(x) \pm T^{\pm}_{0,l}(x)\right], \\ T^{\pm}_{k+1,l}(x) &= 2xT^{\pm}_{k,l}(x) - T^{\pm}_{k,l+1}(x) \\ &\quad- T^{\pm}_{k,|l-1|}(x) \pm 2T^{\pm}_{k,l}(x) - T^{\pm}_{|k-1|,l}(x). \end{aligned} \tag{A14}$$

3. Chebyshev expansion of the convolution

In this subsection, we derive a recurrence relation that allows for efficient evaluation of $t^{j}_{k,l}$ in constant time per coefficient. Let us consider a Chebyshev expansion of Eq. (A14),

$$T^{\pm}_{k,l}(x) = {\sum_{j=0}^{l+k+1}}' t^{j(\pm)}_{k,l} T_j(x). \tag{A15}$$

Summation limit $k+l+1$ comes from the fact that $T_k(x-\tau\pm1)T_l(\tau)$ is a polynomial of degree at most $k+l$ in τ, and the integration in (A2b) and (A2c) adds one to the degree.

First, consider the boundary conditions. In the case of $l=0$, the coefficients $t^{j(\pm)}_{k,0}$ are obtained from the solution of the following equations:

$$\begin{aligned} {\sum_{j=0}^{k+1}}' t^{j(\pm)}_{k,0} T_j(x) &= \frac{T_{k+1}(x)-(\pm1)^{k+1}T_0(x)}{2(k+1)} \\ &\quad- \frac{T_{|k-1|}(x)-(\pm1)^{k-1}T_0(x)}{2(k-1)}(1-\delta_{k,1}). \end{aligned}$$

$k=1$,

$$t^{j(\pm)}_{1,0} = \begin{cases} -\frac{1}{2}, & j=0, \\ \frac{1}{4}, & j=2, \\ 0, & \text{otherwise}. \end{cases}$$

$k \neq 1$,

$$\sum_{j=0}^{k+1}{}' t_{k,0}^{j(\pm)} T_j(x) = \frac{T_{k+1}(x) - (\pm 1)^{k+1} T_0(x)}{2(k+1)} - \frac{T_{|k-1|}(x) - (\pm 1)^{k-1} T_0(x)}{2(k-1)} = \frac{T_{k+1}(x)}{2k+2} - \frac{T_{|k-1|}(x)}{2k-2} + \frac{2(\pm 1)^{k+1}}{k^2-1}\frac{T_0(x)}{2}.$$

By grouping Chebyshev polynomials of the same order, we get the following expressions:

$$t_{k,0}^{j(\pm)} = \begin{cases} \frac{2(\pm 1)^{k+1}}{k^2-1}, & j = 0, \\ -\frac{1}{2k-2}, & j = k-1,\ k > 0, \\ \frac{1}{2k+2}, & j = k+1,\ k > 0, \\ 1, & k = 0,\ j = 1. \end{cases}$$

$l > 0, k = 1$,

$$\sum_{j=0}^{l+2}{}' t_{1,l}^{j(\pm)} T_j(x) = \frac{1}{2}\sum_{j=0}^{l+2}{}' \Big[\frac{t_{0,l}^{j-1(\pm)}}{2^{\delta_{j,1}}}\delta_{j>0} + \frac{1}{2} t_{0,l}^{0(\pm)}\delta_{j,1} + 2^{\delta_{j,0}} t_{0,l}^{j+1(\pm)}\delta_{j\leqslant l} - t_{0,l+1}^{j(\pm)} - t_{0,l-1}^{j(\pm)}\delta_{j\leqslant l} \pm 2 t_{0,l}^{j(\pm)}\delta_{j\leqslant l+1} \Big] T_j(x).$$

General case $l > 0, k > 0$,

$$\sum_{j=0}^{k+l+2}{}' t_{k+1,l}^{j(\pm)} T_j(x) = \sum_{j=0}^{k+l+2}{}' \Big[\frac{t_{k,l}^{j-1(\pm)}}{2^{\delta_{j,1}}}\delta_{j>0} + \frac{1}{2} t_{k,l}^{0(\pm)}\delta_{j,1} + 2^{\delta_{j,0}} t_{k,l}^{j+1(\pm)}\delta_{j\leqslant k+l} - t_{k,l+1}^{j(\pm)} - t_{k,l-1}^{j(\pm)}\delta_{j\leqslant k+l} \pm 2 t_{k,l}^{j(\pm)}\delta_{j\leqslant k+l+1} - t_{k-1,l}^{j(\pm)}\delta_{j\leqslant k+l} \Big] T_j(x).$$

Now we can summarize the results for the $t_{kl}^{j(\pm)}$ coefficients:

$k = 1, l = 0$,

$$t_{1,0}^{j(\pm)} = \begin{cases} -\frac{1}{2}, & j = 0, \\ \frac{1}{4}, & j = 2, \\ 0, & \text{otherwise}. \end{cases} \tag{A16a}$$

$k \neq 1, l = 0$,

$$t_{k,0}^{j(\pm)} = \begin{cases} \frac{2(\pm 1)^{k+1}}{k^2-1}, & j = 0, \\ -\frac{1}{2k-2}, & j = k-1, k > 0, \\ \frac{1}{2k+2}, & j = k+1, k > 0, \\ 1, & k = 0, j = 1. \end{cases} \tag{A16b}$$

$k = 1, l > 0$,

$$t_{1,l}^{j(\pm)} = \frac{1}{2}\frac{t_{0,l}^{j-1(\pm)}\delta_{j>0}}{2^{\delta_{j,1}}} + \frac{t_{0,l}^{0(\pm)}\delta_{j,1}}{2} + 2^{\delta_{j,0}} t_{0,l}^{j+1(\pm)}\delta_{j\leqslant l} - t_{0,l+1}^{j(\pm)} - t_{0,l-1}^{j(\pm)}\delta_{j\leqslant l} \pm 2 t_{0,l}^{j(\pm)}\delta_{j\leqslant l+1}. \tag{A16c}$$

$k > 0, l > 0$,

$$t_{k+1,l}^{j(\pm)} = \frac{t_{k,l}^{j-1(\pm)}\delta_{j>0}}{2^{\delta_{j,1}}} + \frac{t_{k,l}^{0(\pm)}\delta_{j,1}}{2} + 2^{\delta_{j,0}} t_{k,l}^{j+1(\pm)}\delta_{j\leqslant k+l} - t_{k,l+1}^{j(\pm)} - t_{k,l-1}^{j(\pm)}\delta_{j\leqslant k+l} \pm 2 t_{k,l}^{j(\pm)}\delta_{j\leqslant k+l+1} - t_{k-1,l}^{j(\pm)}\delta_{j\leqslant k+l}. \tag{A16d}$$

And the final expression for t-coefficients will be

$$t_{kl}^{j} = t_{kl}^{j(-)} \pm t_{kl}^{j(+)}, \tag{A17}$$

where the plus (minus) sign corresponds to the fermionic (bosonic) convolution.

APPENDIX B: COMPARISON TO THE LEGENDRE BASIS

Reference [27] proposed the use of Legendre polynomials as a basis for Monte Carlo Green's functions. These Green's functions could in principle be adapted to the real materials context. Figure 8 shows the maximum error curves of Fig. 1 in the main text. It is evident that the Legendre basis also converges exponentially, but is substantially less compact than the Chebyshev basis. This is expected from the min-max properties of the Chebyshev polynomials. It is also the expected behavior for core states, as the zeros of the Chebyshev polynomials are closer to -1 and 1 than those of Legendre polynomials of the same order [55], and they are therefore better able to resolve the exponential decay core states and high-lying excitations.

The two types of polynomials differ in several technical aspects. For instance, the roots of Chebyshev polynomials are known analytically, whereas those of Legendre polynomials need to be evaluated numerically and tabulated. On the other hand, the orthogonality relation of the Legendre polynomials is easier.

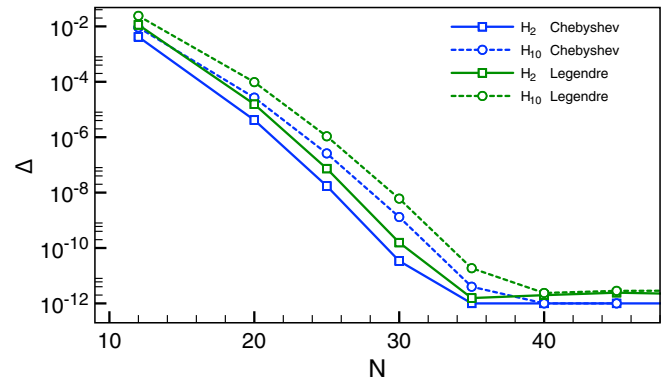

FIG. 8. Convergence of the Hartree-Fock Green's function with the number of Chebyshev and Legendre expansion coefficients. Blue curves correspond to the maximum difference of the Chebyshev expansion when compared to the exact result (Fig. 1). Green curves show the same data, for the Legendre basis [27]. H_2 molecule (open square) and H_{10} chain (open circle) parameters as specified in Table I.

[1] A. A. Abrikosov, I. Dzyaloshinskii, L. P. Gorkov, and R. A. Silverman, *Methods of Quantum Field Theory in Statistical Physics* (Dover, New York, NY, 1975).
[2] C. Bloch and C. D. Dominicis, Nucl. Phys. **7**, 459 (1958).
[3] J. M. Luttinger and J. C. Ward, Phys. Rev. **118**, 1417 (1960).
[4] D. Bohm and D. Pines, Phys. Rev. **92**, 609 (1953).
[5] M. Gell-Mann and K. A. Brueckner, Phys. Rev. **106**, 364 (1957).
[6] N. E. Dahlen and R. van Leeuwen, J. Chem. Phys. **122**, 164102 (2005).
[7] J. J. Phillips and D. Zgid, J. Chem. Phys. **140**, 241101 (2014).
[8] J. J. Phillips, A. A. Kananenka, and D. Zgid, J. Chem. Phys. **142**, 194108 (2015).
[9] A. A. Kananenka, J. J. Phillips, and D. Zgid, J. Chem. Theor. Comput. **12**, 564 (2016).
[10] A. A. Kananenka, A. R. Welden, T. N. Lan, E. Gull, and D. Zgid, J. Chem. Theor. Comput. **12**, 2250 (2016).
[11] A. A. Rusakov and D. Zgid, J. Chem. Phys. **144**, 054106 (2016).
[12] A. R. Welden, A. A. Rusakov, and D. Zgid, J. Chem. Phys. **145**, 204106 (2016).
[13] L. Hedin, Phys. Rev. **139**, A796 (1965).
[14] R. Blankenbecler, D. J. Scalapino, and R. L. Sugar, Phys. Rev. D **24**, 2278 (1981).
[15] J. E. Hirsch and R. M. Fye, Phys. Rev. Lett. **56**, 2521 (1986).
[16] A. N. Rubtsov, V. V. Savkin, and A. I. Lichtenstein, Phys. Rev. B **72**, 035122 (2005).
[17] P. Werner, A. Comanac, L. de'Medici, M. Troyer, and A. J. Millis, Phys. Rev. Lett. **97**, 076405 (2006).
[18] E. Gull, P. Werner, O. Parcollet, and M. Troyer, Europhys. Lett. **82**, 57003 (2008).
[19] E. Gull, A. J. Millis, A. I. Lichtenstein, A. N. Rubtsov, M. Troyer, and P. Werner, Rev. Mod. Phys. **83**, 349 (2011).
[20] N. Prokof'ev and B. Svistunov, Phys. Rev. Lett. **99**, 250201 (2007).
[21] A. Georges, G. Kotliar, W. Krauth, and M. J. Rozenberg, Rev. Mod. Phys. **68**, 13 (1996).
[22] A. Toschi, A. A. Katanin, and K. Held, Phys. Rev. B **75**, 045118 (2007).
[23] A. N. Rubtsov, M. I. Katsnelson, and A. I. Lichtenstein, Phys. Rev. B **77**, 033101 (2008).
[24] T. Maier, M. Jarrell, T. Pruschke, and M. H. Hettler, Rev. Mod. Phys. **77**, 1027 (2005).
[25] W. Ku, Ph.D. thesis, University of Tennessee, 2000.
[26] W. Ku and A. G. Eguiluz, Phys. Rev. Lett. **89**, 126401 (2002).
[27] L. Boehnke, H. Hafermann, M. Ferrero, F. Lechermann, and O. Parcollet, Phys. Rev. B **84**, 075145 (2011).
[28] J. Otsuki, M. Ohzeki, H. Shinaoka, and K. Yoshimi, Phys. Rev. E **95**, 061302 (2017).
[29] H. Shinaoka, J. Otsuki, M. Ohzeki, and K. Yoshimi, Phys. Rev. B **96**, 035147 (2017).
[30] J. C. Mason and D. C. Handscomb, *Chebyshev Polynomials* (CRC, Boca Raton, FL, 2003).
[31] W. H. Press, S. A. Teukolsky, W. T. Vetterling, and B. P. Flannery, *Numerical Recipes in FORTRAN; The Art of Scientific Computing*, 2nd ed. (Cambridge University Press, New York, 1993).
[32] C. W. Clenshaw, Math. Comp. **9**, 118 (1955).
[33] N. Hale and A. Townsend, SIAM J. Sci. Comput. **36**, A1207 (2014).
[34] S. Zemyan, *The Classical Theory of Integral Equations: A Concise Treatment*, SpringerLink: Bücher (Birkhäuser, Boston, 2012).
[35] N. Säkkinen, Y. Peng, H. Appel, and R. van Leeuwen, J. Chem. Phys. **143**, 234101 (2015).
[36] A.-B. Comanac, Ph.D. thesis, Columbia University, 2007.
[37] A. A. Rusakov, J. J. Phillips, and D. Zgid, J. Chem. Phys. **141**, 194105 (2014).
[38] A. S. Fokas and S. A. Smitheman, arXiv:1211.4943 (math.NA).
[39] V. Domínguez, I. G. Graham, and V. P. Smyshlyaev, IMA J. Numer. Anal. **31**, 1253 (2011).
[40] A. Szabo and N. Ostlund, *Modern Quantum Chemistry: Introduction to Advanced Electronic Structure Theory*, Dover Books on Chemistry (Dover, Mineola, NY, 1996).
[41] F. David, J. Comput. Chem. **17**, 1571 (1996).
[42] K. L. Schuchardt, B. T. Didier, T. Elsethagen, L. Sun, V. Gurumoorthi, J. Chase, J. Li, and T. L. Windus, J. Chem. Inf. Model. **47**, 1045 (2007).
[43] W. J. Hehre, R. F. Stewart, and J. A. Pople, J. Chem. Phys. **51**, 2657 (1969).
[44] M. F. Peintinger, D. V. Oliveira, and T. Bredow, J. Comput. Chem. **34**, 451 (2013).
[45] P. J. Hay and W. R. Wadt, J. Chem. Phys. **82**, 270 (1985).
[46] W. R. Wadt and P. J. Hay, J. Chem. Phys. **82**, 284 (1985).
[47] P. J. Hay and W. R. Wadt, J. Chem. Phys. **82**, 299 (1985).
[48] R. Nada, J. B. Nicholas, M. I. McCarthy, and A. C. Hess, Int. J. Quantum Chem. **60**, 809 (1996).
[49] B. Civalleri and P. Ugliengo, J. Phys. Chem. B **104**, 9491 (2000).
[50] M. Prencipe, Y. Noel, B. Civalleri, C. Roetti, and R. Dovesi, Phys. Chem. Miner. **33**, 519 (2006).
[51] N. Chikano, J. Otsuki, and H. Shinaoka, Phys. Rev. B **98**, 035104 (2018).
[52] K. A. Peterson, D. Figgen, E. Goll, H. Stoll, and M. Dolg, J. Chem. Phys. **119**, 11113 (2003).
[53] K. A. Peterson, J. Chem. Phys. **119**, 11099 (2003).
[54] A. Stan, N. E. Dahlen, and R. van Leeuwen, J. Chem. Phys. **130**, 114105 (2009).
[55] G. Szego, Trans. Am. Math. Soc. **39**, 1 (1936).